A New Model Predictive Current Controller for Grid-Connected Converters in Unbalanced Grids

Euan T. Andrew, *Student Member, IEEE*, Khaled H. Ahmed, *Senior Member, IEEE*, and Derrick Holliday

***Abstract*—Distributed energy resources are often connected to low-voltage distribution networks where the grid voltages may be unbalanced. This leads to an unwanted ripple in the output active power at twice the fundamental grid frequency. In this article, a new model predictive current controller is proposed for unbalanced grids. The variable switching frequency of existing model predictive controllers is fixed and the power quality is improved. A Kalman filter estimator is used to extract the positive and negative sequence components. A new calculation time compensation technique is proposed, which offers superior accuracy to existing approaches. A grid voltage discretization compensation strategy is outlined, and its effectiveness is demonstrated. Finally, the system stability is verified theoretically. Simulation and laboratory results are included to prove the robustness of the proposed controller and support the theoretical analysis.**

***Index Terms*—Current control, grid connected, modulated model predictive control, voltage source converter.**

I. Introduction

THE drive to integrate more renewables into utility grids means that the number of grid-connected power converters continues to increase [1], [2]. These distributed energy resources are often connected to low-voltage distribution networks, where the voltage may be unbalanced at the terminals of the grid-connected converters [3]. Unbalanced grid voltages lead to unwanted ripple in the active power output. Therefore, the current controller used in the interfacing converter must be able to deal with unbalanced grid conditions.

Vector current controllers (VCC) are widely used in grid-connected applications due to their good steady-state accuracy [4]; however, their dynamic performance is slow compared to advanced techniques [5]. VCC strategies for unbalanced grids rely on splitting the current controller into separate positive and negative sequence frames [6], which doubles the number of PI controllers [7], leading to tuning difficulty. In addition, VCCs operate in a synchronous reference frame, therefore, they require a phase-locked loop (PLL) to synchronize with the grid [3]. The behavior of the current controller and PLL are linked, making their design challenging [8], [9]. The PLL must perform well during symmetrical and asymmetrical operation [3], and the PLL topologies proposed for unbalanced grids are often highly complex and require difficult tuning procedures to achieve good accuracy and acceptable stability margin [10].

Model predictive control (MPC) is a promising alternative to VCC, where a predictive model is used to select the optimum control sequence [11]. Finite control set MPC (FCS-MPC) has been widely used but the switching frequency is variable, which leads to poor power quality. The computational burden of this approach has been criticized [12], [13] since all available voltage vectors are evaluated when only one is actually required [14], [15]. In [15], a reference voltage vector is calculated to allow the best active vector to be identified without exhaustive evaluation. However, an additional deadbeat control stage is required. In [16], a low-complexity model predictive power control (LC-MPPC) approach was proposed, where the negative complex conjugate of the power is selected as the control variable, and the vector that minimizes the power error is selected directly. However, the variable switching frequency problem of FCS-MPC remains. In [17], the LC-MPPC was improved by switching between the active vector and a zero vector and in [18], a second active vector may be selected instead of a zero vector to further reduce the error. This achieves a fixed switching frequency, however, since only two vectors are applied, a complete range of output voltages cannot be synthesized and the zero steady-state error cannot be achieved. Furthermore, since LC-MPPC uses the negative complex conjugate of the power as the control variable, the controller output currents are highly distorted for unbalanced grids, where the definition of complex power is not valid. Alternatively, in [19], the FCS-MPC technique was enhanced by adding a discrete space vector modulator (DSVM) and defining additional virtual voltage vectors, which the algorithm may select. The resulting technique is known as MPC-DSVM. However, these virtual voltage vectors must also be evaluated exhaustively, increasing the computation time significantly even in the simplest case where only 12 additional vectors are defined. Recently, in [20], a deadbeat control stage has been used to calculate the approximate output voltage, then, floating virtual voltage vectors (FVVV-MPC) are defined close to the approximate value and are evaluated based on a cost function. However, with these virtual vector techniques, the range of possible output voltages is still not continuous. Modulated MPC (MMPC) has been proposed to overcome the variable switching frequency and poor steady-state behavior of existing MPC techniques [21]. In MMPC, a modulator exchanges between two

Manuscript received July 29, 2021; revised November 18, 2021 and January 23, 2022; accepted February 24, 2022. Date of publication March 9, 2022; date of current version April 28, 2022. Recommended for publication by Associate Editor F. Dijkhuizen. *(Corresponding author: Euan T. Andrew.)*

The authors are with the Department of Electronic and Electrical Engineering, University of Strathclyde, G1 1XQ Glasgow, U.K. (e-mail: euan.andrew@strath.ac.uk; khaled.ahmed@strath.ac.uk; derrick.holliday@strath.ac.uk).

Color versions of one or more figures in this article are available at https://doi.org/10.1109/TPEL.2022.3158016.

Digital Object Identifier 10.1109/TPEL.2022.3158016

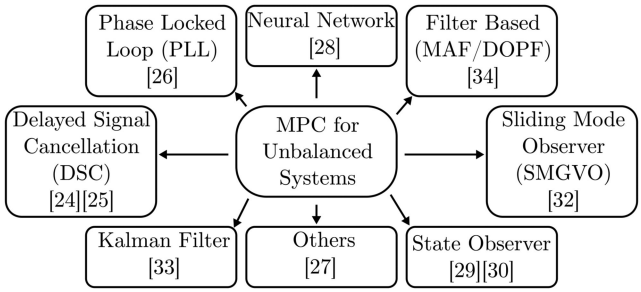

Fig. 1. Overview of symmetrical component extraction techniques for MPC controllers.

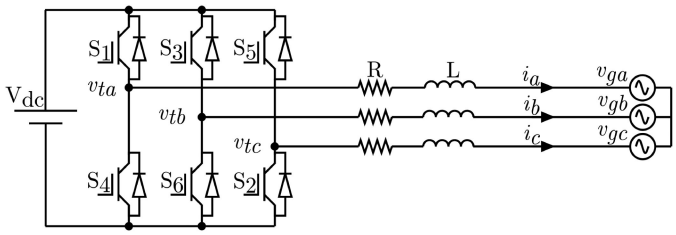

Fig. 2. Two-level grid-connected VSC.

active and two zero vectors to achieve a deadbeat response with a fixed switching frequency, however, the computational burden is high. In [22], MMPC was extended into the overmodulation region. The resulting controller achieves a deadbeat response in the linear region and tends toward the FCS-MPC case in the overmodulation region, which is known to be optimal. This approach is refined in [12], where Pythagoras theorem was used to remove trigonometric functions from the controller to improve the performance on DSPs. However, the computational burden remains high.

For unbalanced grid operation, the symmetrical component approach is the most common technique and many methods have been proposed to extract the symmetrical components [23]. An overview is provided in Fig. 1. MPC controllers have been proposed using delayed signal cancellation (DSC) [24], [25]. However, the delay makes it unattractive for situations with a high current control bandwidth. To avoid the drawbacks of DSC, MPC current controllers have been proposed using PLLs [26], [27]. This introduces all the challenges of PLL design to a system, which would otherwise operate entirely in a stationary frame. In [28], a predictive controller was proposed using a neural network to separate the sequence components, however, the learning rate must be tuned carefully and many trigonometric calculations are required. In [29] and [30], state observers were employed. However, the system is complex and the gains must be tuned carefully to ensure stability [31]. In [32], a sliding-mode grid voltage observer for unbalanced grids was proposed, however, a frequency-locked loop (FLL) is required, which brings all the well-known challenges of FLLs [31]. In [33], a new state-space formulation of the symmetrical component extraction problem has been developed and an extended complex Kalman filter (ECKF) was proposed to estimate the symmetrical components even in noisy systems. Moreover, the ECKF estimator compares well with the techniques examined in [34], where the response times of dual second-order generalized integrator, moving average filter, DSC, and delay operation period filter-based techniques are estimated.

This article proposes a new MMPC implementation, which uses the direction of the current reference vector to select the active vectors, reducing the computational burden by half with no degradation in the performance. Furthermore, an ECKF is included to estimate the symmetrical components of the grid voltage with improved noise immunity, allowing the proposed MMPC current controller to be extended to an unbalanced system. Moreover, the ECKF is modified to predict the grid voltage two steps in advance, thereby providing a new computation time compensation technique and removing the need for the Lagrange extrapolation. The effects of parameter mismatch and grid voltage discretization are examined, and a compensation strategy is proposed. Compared with the existing literature, this proposed control system offers the following advantages.

1) The proposed MMPC active vectors are selected without incurring the computational burden of existing exhaustive evaluation techniques.
2) The symmetrical components are estimated accurately without a PLL, avoiding tuning and delay issues.
3) The proposed modified ECKF estimator achieves superior noise rejection compared with existing DSC techniques.
4) The controller computation time is compensated without relying on a Lagrange extrapolation, improving the transient and steady-state behavior.
5) The effects of grid voltage discretization are fully analyzed and compensated to reduce the steady-state error.

The rest of this article is organized as follows. Section II derives the new MPC equations. Section III describes the modified ECKF estimator. Section IV describes the proposed control system. Section V studies the effects of parameter mismatch and grid voltage discretization and proposes a compensation method. Section VI verifies that the proposed controller is stable in the sense of Lyapunov in the vicinity of the steady state. Section VII studies the proposed control system in simulation and compares it with two existing MPC controllers. Section VIII includes the results of the experimental validation. Section IX compares the computational burden of the proposed technique and the conventional MPC. Finally, Section X concludes this article.

II. Proposed Modulated Model Predictive Current Controller

This section describes an alternative implementation of MMPC current control offering reduced computational burden without sacrificing the system performance.

A. Mathematical Model of a Two-Level VSC

A circuit diagram of a grid-connected VSC interfaced via an L-filter is provided in Fig. 2

$$\begin{bmatrix} v_{t\alpha} \\ v_{t\beta} \end{bmatrix} = \begin{bmatrix} v_{g\alpha} \\ v_{g\beta} \end{bmatrix} + R \begin{bmatrix} i_\alpha \\ i_\beta \end{bmatrix} + L \frac{d}{dt} \begin{bmatrix} i_\alpha \\ i_\beta \end{bmatrix} \tag{1}$$

where $v_{g\alpha}$ and $v_{g\beta}$ are the stationary components of the grid voltage, i_α and i_β are the stationary components of the grid current, and R and L are the resistance and inductance of the

interfacing filter, respectively. The current derivative can be approximated using a forward Euler method

$$\frac{di_\alpha}{dt} \approx \frac{i_{\alpha(k+1)} - i_{\alpha(k)}}{T_s} \tag{2}$$

where $i_{\alpha(k+1)}$ is the grid current sampled at instant $k+1$, $i_{\alpha(k)}$ is the grid current sampled at instant k, and T_s is the sampling time. Substituting (2) into (1) yields a discrete predictive model describing the future grid current as a function of the proposed terminal voltage

$$\begin{bmatrix} i_{\alpha(k+1)} \\ i_{\beta(k+1)} \end{bmatrix} = \left(1 - R\frac{T_s}{L}\right) \begin{bmatrix} i_{\alpha(k)} \\ i_{\beta(k)} \end{bmatrix} + \frac{T_s}{L}\left(\begin{bmatrix} v_{t\alpha(k)} \\ v_{t\beta(k)} \end{bmatrix} - \begin{bmatrix} v_{g\alpha(k)} \\ v_{g\beta(k)} \end{bmatrix} \right). \tag{3}$$

B. Calculation of Duty Factors

The current controller must select an optimum voltage vector v_{opt} and second-best vector v'_{opt} and switch between them and the zero vectors to synthesize the terminal voltage, which minimizes the current error. Within the linear modulation region, the current error should be reduced to zero by the end of the sampling period, according to the principle of deadbeat control. The duty factors for the active and zero vectors can be found by solving the following system of equations:

$$i_\alpha^{v_{\text{opt}}} d_1 + i_\alpha^{v'_{\text{opt}}} d_2 + i_\alpha^{v_0} d_0 = i_\alpha^* \tag{4}$$

$$i_\beta^{v_{\text{opt}}} d_1 + i_\beta^{v'_{\text{opt}}} d_2 + i_\beta^{v_0} d_0 = i_\beta^* \tag{5}$$

$$d_1 + d_2 + d_0 = 1 \tag{6}$$

where $i_\alpha^{v_{\text{opt}}}$, $i_\alpha^{v'_{\text{opt}}}$, and $i_\alpha^{v_0}$ are the currents, which would result from applying v_{opt}, v'_{opt} or either of the zero vectors for one whole sampling period, respectively, and d_1, d_2, and d_0 are the duty factors for the active and zero vectors, respectively.

C. Selection of Active Vectors

In a typical MMPC implementation [21], the two active vectors are selected by evaluating the predictive model (3) exhaustively for all six output states and comparing the predicted current with the reference. It is common practice to solve the control problem, a step in advance to compensate for the calculation time. Therefore, the cost function is designed to calculate the predicted error at instant $k+2$, to select the optimum vector to apply at $k+1$. Typically, a quadratic cost function is used as follows:

$$G_x = \left[i^*_{\alpha\beta(k+2)} - i^{v_x}_{\alpha\beta(k+2)} \right]^2, x \in [0,7] \tag{7}$$

where $i^{v_x}_{\alpha\beta(k+2)}$ is the current predicted two steps in advance for each of the eight voltage vectors. The errors G_x are sorted, and the best and second-best vectors are selected. Therefore, (3) and (7) must be evaluated 6 times, even though only two vectors will be used. Fig. 3 shows the output voltage vectors for a two-level VSC, together with their predicted currents. An arbitrary current reference vector is also included. To reduce the computational burden of selecting the active vectors, the angle of the reference current vector may be used. The vectors v_{opt} and v'_{opt} should be those producing currents, which are geometrically closest and second closest to the current reference vector. Since the predicted current hexagon of Fig. 3 is not centered at zero, a complex direction vector is first calculated as

$$i^*_{\text{dir}} = i^*_{\alpha\beta(k+2)} - i^{v_0}_{\alpha\beta(k+2)} \tag{8}$$

where $i^*_{\alpha\beta(k+2)}$ is the reference current vector at instant $k+2$ and $i^{v_0}_{\alpha\beta(k+2)}$ is the current predicted for instant $k+2$ if v_0 is applied. The active vectors can then be easily identified by determining, which quadrant the direction vector points to using simple compare-to-zero operations. Fig. 4(a) shows an example current reference direction vector. Considering the alpha and beta components of $i^{\text{dir}}_{\alpha\beta}$ separately, if $i^{\text{dir}}_\alpha > 0$ and $i^{\text{dir}}_\beta > 0$, then the direction vector points to the first quadrant. The quadrant is further divided into subsectors "A," "B," and "C." The exact values of the tangent function can then be exploited using compare-to-constant operations to determine which subsector the direction vector lies in, thereby identifying v_{opt} and v'_{opt}, as shown in Fig. 4(a). For example, if

$$\frac{i^*_{\text{dir}\alpha}}{i^*_{\text{dir}\beta}} > \frac{\sqrt{3}}{3} \tag{9}$$

then the direction vector points to subsector "B" and vectors v^2 and v^1 should be selected as v_{opt} and v'_{opt}, respectively. A similar method may be applied to all other quadrants and sectors. This technique selects precisely the same vectors as an exhaustive

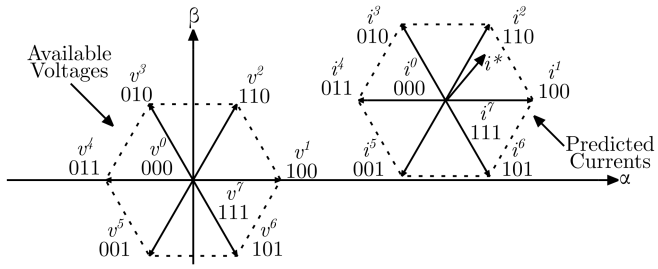

Fig. 3. Available voltage vectors and their resulting predicted currents.

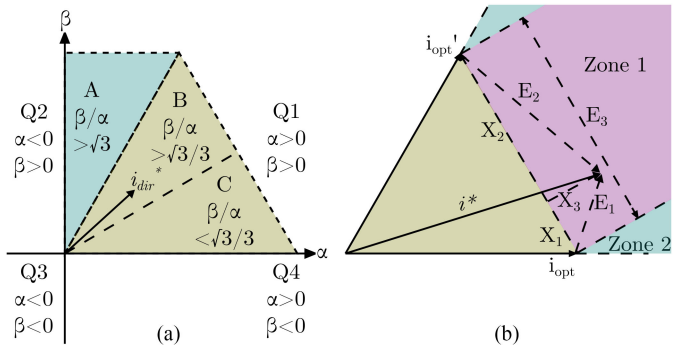

Fig. 4. Quadrant and subsector identification in (a) linear region and (b) overmodulation region.

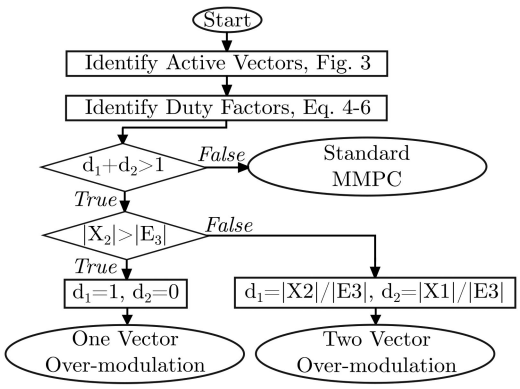

Fig. 5. Flowchart of the proposed MMPC algorithm with optimized overmodulation.

search but with much less computation since the exact values of the tangent function may be calculated offline.

D. Extension to the Overmodulation Region

During large changes in the converter operating conditions, the current controller may be unable to track the reference within one sampling period due to the limitation of the available dc voltage. Under these conditions, the current reference vector lies outside the predicted current hexagon, as shown in Fig. 3, and (4)–(6) yield an infeasible solution where $d_1 + d_2 > 1$. The theoretical basis for the overmodulation method was examined fully in [22] and is repeated here only insofar as is necessary to explain the proposed simplification. Fig. 4(b) shows a current reference vector, which lies outside the linear modulation region. In Zone 1, vector arithmetic is used to determine the optimum ratio of v_{opt} and v'_{opt} to minimize the current error. In Zone 2, v_{opt} should be applied for the whole sampling period. The vectors $E_{1,2,3}$ are given by

$$E_1 = i^* - i_{\text{opt}} \tag{10}$$

$$E_2 = i^* - i'_{\text{opt}} \tag{11}$$

$$E_3 = i'_{\text{opt}} - i_{\text{opt}}. \tag{12}$$

Using the Pythagoras theorem, the magnitudes of vectors $X_{1,2,3}$ are given by

$$|X_1| = \frac{1}{2}\left(\frac{|E_1|^2 - |E_2|^2 + |E_3|^2}{|E_3|}\right) \tag{13}$$

$$|X_2| = \frac{1}{2}\left(\frac{|E_2|^2 - |E_1|^2 + |E_3|^2}{|E_3|}\right). \tag{14}$$

In both [22] and [12], checks were performed to see whether the current reference lies closer to i_{opt} or i'_{opt}. However, this is unnecessary, since if the reference vector was closer to i'_{opt} then clearly i'_{opt} would have been selected as i_{opt} in the first place. The overmodulation algorithm can, therefore, be simplified, as shown in Fig. 5, where only two comparison operations are required to identify, which modulation scenario is required. One to establish whether overmodulation is required and another to establish whether one active or two active vectors must be used.

III. Modified ECKF

This section describes the proposed ECKF, which is used to extract the instantaneous symmetrical components of the grid voltage. Furthermore, a modification is proposed, where new equations are added to the Kalman filter to estimate the voltages two steps in advance to compensate for the calculation time. The positive and negative sequence components of the grid voltage can be expressed in complex exponential form as follows:

$$V^+ = v_\alpha^+ + jv_\beta^+ = A^+ e^{j\omega k T_s} \tag{15}$$

$$V^- = v_\alpha^- + jv_\beta^- = A^- e^{-j\omega k T_s}. \tag{16}$$

The behavior of the grid voltages over time can be described by a discrete-state space model of the form

$$X_{(k+1)} = A_d X_{(k)} \tag{17}$$

where the state vector $X_{(k)}$ is given by

$$X_{(k)} = \begin{bmatrix} x_{0(k)} \\ x_{1(k)} \\ x_{2(k)} \end{bmatrix} = \begin{bmatrix} e^{j\omega T_s} \\ A^+ e^{j\omega k T_s} \\ A^- e^{-j\omega k T_s} \end{bmatrix} \tag{18}$$

and the discrete state transition matrix A_d is given by

$$A_d = \begin{bmatrix} 1 & 0 & 0 \\ 0 & x_{0(k)} & 0 \\ 0 & 0 & \frac{1}{x_{0(k)}} \end{bmatrix}. \tag{19}$$

A. Conventional ECKF

The ECKF requires the system to be described by a nonlinear state transition model and a measurement model as follows:

$$\begin{aligned} X_{(k+1)} &= f\left(X_{(k)}, u_{(k)}\right) + w_{(k-1)} \\ &= A_d X_{(k)} + w_{(k-1)} \end{aligned} \tag{20}$$

$$z_{(k)} = h\left(X_{(k)}\right) + v_{(k)} \tag{21}$$

where $f(X_{(k)}, u_{(k)})$ is a nonlinear function relating the future state $X_{(k+1)}$ to the current state $X_{(k)}$ and current inputs $u_{(k)}$, and $h(X_{(k)}) + v_{(k)}$ is a nonlinear function relating the current measurement $z_{(k)}$ to the current state $X_{(k)}$. Also, $w_{(k-1)}$ and $v_{(k)}$ are zero-mean Gaussian noises describing the noise in the process and measurement models, with covariance matrices Q and R, respectively. The ECKF linearizes the system around the previous state estimate. This involves computing the first-order partial derivatives of the process and measurement matrices at each time step. The Jacobians are calculated using

$$F_{(k-1)} = \frac{\partial f}{\partial X}\Big|_{\substack{X=\hat{X}^+_{(k-1)} \\ u=u_{(k-1)}}} \tag{22}$$

$$H_{(k)} = \frac{\partial h}{\partial X}\Big|_{X=\hat{X}^-_{(k)}} \tag{23}$$

where $H_{(k)}$ is the linearized measurement matrix and $F_{(k-1)}$ is the linearized state transition matrix. Applying (22) and (23)

to the nonlinear state-space model of (20) and (21) yields the system and measurement matrices linearized about the current state estimate, as required for the Kalman filter prediction and update equations. The ECKF can then be implemented using the following equations for the prediction stage:

$$\hat{X}^{-}_{(k)} = f\left(\hat{X}^{+}_{(k-1)}, u_{(k-1)}\right) \tag{24}$$

$$P^{-}_{(k)} = F_{(k-1)}P^{+}_{(k-1)}F^{T}_{(k-1)} + Q \tag{25}$$

$$K_{(k)} = P^{-}_{(k)}H^{T}_{(k)}\left(R + H_{(k)}P^{-}_{(k)}H^{T}_{(k)}\right)^{-1} \tag{26}$$

where $\hat{X}^{-}_{(k)}$ is the uncorrected state estimate, $f(\hat{X}^{+}_{(k-1)}, u_{(k-1)})$ is the nonlinear system model, $P^{-}_{(k)}$ is the uncorrected state error covariance matrix, $P^{+}_{(k-1)}$ is the corrected state error covariance matrix, and $K_{(k)}$ is the Kalman gain. At every iteration, the uncorrected state updates are corrected using the latest measurements.

B. Modified ECKF

If the system is sampled at instant k, by the time when the necessary calculations have been performed, the control decision may be out of date when it is applied. To compensate for this, the controller may extrapolate future quantities and instead solve for the optimum control action to be applied at instant $k+1$ to minimize the cost function at $k+2$. A modification to the ECKF is proposed to also estimate the grid voltage at instants $k+1$ and $k+2$. The change in the state variables over time is described by (17). Since the system state at instant k has already been estimated, (17) can be used to advance the estimates by one time step as follows:

$$\hat{X}^{+}_{(k+1)} = A_d\hat{X}^{+}_{(k)}. \tag{27}$$

Similarly, advancing (17) by one time step and substituting for (27) gives

$$\hat{X}^{+}_{(k+2)} = A_d\hat{X}^{+}_{(k+1)} = A^2_d\hat{X}^{+}_{(k)}. \tag{28}$$

With these new equations added, the update equations of the modified ECKF are

$$\tilde{y}_{(k)} = z_{(k)} - h\left(\hat{X}^{-}_{(k)}\right) \tag{29}$$

$$\hat{X}^{+}_{(k)} = \hat{X}^{-}_{(k)} + K_{(k)}\tilde{y}_{(k)} \tag{30}$$

$$P^{+}_{(k)} = \left(I - K_{(k)}H_{(k)}P^{-}_{(k)}\right). \tag{31}$$

If Q is increased, $P^{-}_{(k)}$ will increase; therefore, the Kalman gain $K_{(k)}$ will increase as well. This means less emphasis is placed on the predictive model and changes in the measurements will be reflected more quickly in the estimated voltages, but more measurement noise will be observed on the estimator outputs. Similarly, if R is increased, the Kalman gain $K_{(k)}$ will decrease. Thus, more emphasis is placed on the latest measurements leading to more noise propagating through to the estimator output. However, the response to changes in the measurements will be faster. Q and R are determined empirically as

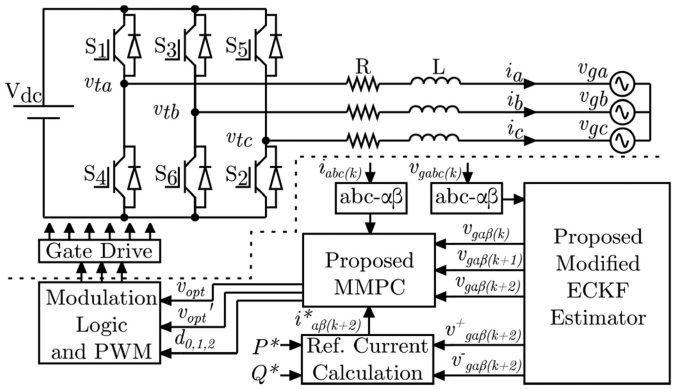

Fig. 6. Complete MPC control system.

$$Q = \begin{bmatrix} 0 & 0 & 0 \\ 0 & 0.01 & 0 \\ 0 & 0 & 0.01 \end{bmatrix} \tag{32}$$

$$R = [5 + j5]. \tag{33}$$

Furthermore, since the new equations calculate the grid voltage two steps in advance, the current references can be calculated directly for instant $k+2$. This removes the need to extrapolate the current references, further improving the noise rejection of the controller. Moreover, the estimated future grid voltages are used in the grid voltage discretization technique described in Section V.

IV. Proposed Control System

A complete MPC system is proposed to regulate the active and reactive power exchanged between a grid-connected converter and an unbalanced grid. The system diagram is shown in Fig. 6.

A. Current Reference Generation

To export the required active and reactive power into the grid, the reference currents must be calculated as a function of the grid voltage as described in [35]. The modified ECKF estimates the grid voltage at instant $k+2$; therefore, the current references may be calculated directly for instant $k+2$. The references are calculated to prevent oscillation of the active power as follows:

$$i^{*+}_{\alpha(k+2)} = \frac{P^{*}v^{+}_{g\alpha(k+2)}}{A} + \frac{Q^{*}v^{+}_{g\beta(k+2)}}{B} \tag{34}$$

$$i^{*+}_{\beta(k+2)} = \frac{P^{*}v^{+}_{g\beta(k+2)}}{A} - \frac{Q^{*}v^{+}_{g\beta(k+2)}}{A} \tag{35}$$

$$i^{*-}_{\alpha(k+2)} = -\frac{P^{*}v^{-}_{g\alpha(k+2)}}{A} + \frac{Q^{*}v^{-}_{g\beta(k+2)}}{A} \tag{36}$$

$$i^{*-}_{\beta(k+2)} = -\frac{P^{*}v^{-}_{g\beta(k+2)}}{A} - \frac{Q^{*}v^{-}_{g\alpha(k+2)}}{A}$$

$$\text{where} \quad A = \left[\left(v^{+}_{g\alpha(k+2)}\right)^2 + \left(v^{+}_{g\beta(k+2)}\right)^2\right] - \left[\left(v^{-}_{g\alpha(k+2)}\right)^2 + \left(v^{-}_{g\beta(k+2)}\right)^2\right]$$
$$B = \left[\left(v^{+}_{g\alpha(k+2)}\right)^2 + \left(v^{+}_{g\beta(k+2)}\right)^2\right] + \left[\left(v^{-}_{g\alpha(k+2)}\right)^2 + \left(v^{-}_{g\beta(k+2)}\right)^2\right] \tag{37}$$

where $v^{+}_{g\alpha(k+2)}$ and $v^{+}_{g\beta(k+2)}$ are the positive sequence components of the grid voltage at instant $k+2$, $v^{-}_{g\alpha(k+2)}$, and $v^{-}_{g\beta(k+2)}$ are the negative sequence components of the grid voltage at instant $k+2$ and P^* and Q^* are the active and reactive power references, respectively.

V. Impact of Parameter Mismatch and Discretization

The effectiveness of any MPC scheme is governed by the accuracy of the predictive model used. The predictive current formula (3) is widely accepted in the literature and has been used in many MPC implementations. However, there are few significant assumptions made, namely the following.

1) The modeled parameters L and R used in the controller are equal to their actual values in the real system.
2) The current derivative is accurately approximated by the forward Euler method.
3) The grid voltage is constant during the sample period.

The impact of parameter mismatch was explored in [36], where a range of incorrect inductance and resistance values were inserted into the predictive model (3) and the resulting erroneous predictions are compared with predictions using the same formula but with the actual values of L and R. The minimum error occurs where L and R used in the predictive formula are equal to their actual values. However, this existing work does not consider the effects of grid voltage discretization and the accuracy of the forward Euler approximation. These combined effects have not been investigated properly for MPC systems in the literature. Fig. 7(a) shows the effect of a similar parameter mismatch on the MPC proposed in this article. The modeled inductance and resistance R_0 and L_0 are kept constant inside the controller, while the actual values in the real system, R and L, are varied. The actual measured output current of the proposed MPC is compared with the current references given by (34)–(37). This ensures that the effects of changing grid voltage and the Euler approximation are also exposed. The steady-state error is calculated as follows:

$$\text{SSE}_{\%} = \sqrt{\frac{1}{N}\sum_{k=1}^{N}\left(i^{*}_{a(k)} - i_{a(k)}\right)^2} * 100\% \tag{38}$$

where N is the number of samples and phase "a" is used for the calculations. Changing the real inductance above or below its modeled value inside the controller leads to an increase in the steady-state error. This is expected since an incorrect inductance will lead to an incorrect output voltage being calculated. The resistance mismatch effect is minimal since the resistance is an order of magnitude smaller than the inductive reactance at the grid frequency. Inspection of Fig. 7(a) suggests that the steady-state error is minimized when the actual inductance of the real system L is less than its modeled value inside the controller L_0. This differs from the previous conclusion in [36] since, in this case, the actual current is compared with the reference current, therefore, the accuracy of the Euler approximation and the effect of grid voltage discretization are also considered.

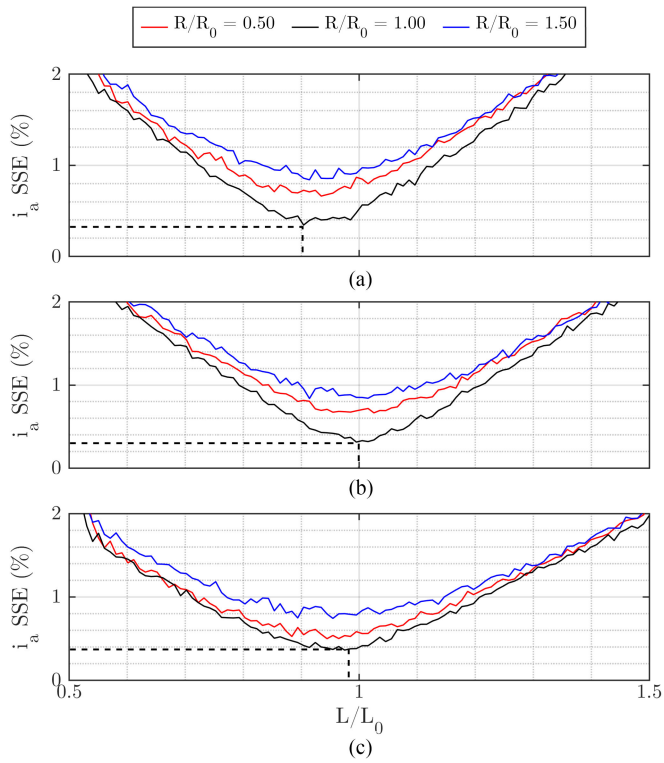

Fig. 7. Steady-state current error when the resistance and inductance of the actual system are varied from 0.5 to 1.5 p.u. while the values used inside the controller are kept constant. The system parameters are as shown in Table I. The error is plotted as a function of the mismatch where (a) grid voltage discretization is not compensated, (b) grid voltage discretization is compensated exactly using (40), and (c) grid voltage discretization is compensated approximately using the method proposed in (41).

The predictive model of (3) assumes that the grid voltage is constant during the sampling period. In fact, the grid voltage is a continuous sinusoidal waveform. It is possible to obtain an exact analytical expression for the predicted grid current by solving the continuous differential equation of (1). Taking the alpha component as an example, a sinusoidal grid voltage is assumed, given by

$$v_{g\alpha}(t) = V^{\text{pk}}_{g\alpha}\sin(\omega t + \omega t_o) \tag{39}$$

where $V^{\text{pk}}_{g\alpha}$ is the peak grid voltage, ω is the angular frequency of the grid, and t_0 is an initial time corresponding to the instantaneous phase angle of the grid. This grid voltage is substituted into the differential equation (1) and the equation is solved for

time $t = T_s$, as shown in the following equation:

$$i_{\alpha(k+1)} = e^{-\frac{RT_s}{L}} \left(i_{\alpha(k)} - \frac{R^2 v_{t\alpha(k)} - R^2 v_{g\alpha}^{\text{pk}} \sin(\omega t_0)}{R(L^2\omega^2 + R^2)} + \frac{L^2 v_{t\alpha(k)}\omega^2 + LRv_{g\alpha}^{\text{pk}}\omega\cos(\omega t_0)}{R(L^2\omega^2 + R^2)} \right) + \left(\frac{R^2 v_{t\alpha(k)} + L^2 v_{t\alpha(k)}\omega^2 - R^2 v_{g\alpha}^{\text{pk}} \sin(\omega t + \omega t_0)}{R(L^2\omega^2 + R^2)} + \frac{LRv_{g\alpha}^{\text{pk}}\cos(\omega t + \omega t_0)}{R(L^2\omega^2 + R^2)} \right). \quad (40)$$

Fig. 7(b) shows that the current error is minimized when the precise predictive formula (40) is used in place of (3) in the controller and R and L are perfectly matched with their correct values in the real system. However, evaluating (40) requires knowledge of the angular velocity of the grid voltage ω, the peak value of the grid voltage $V_{g\alpha}^{\text{pk}}$, and the instantaneous phase of the grid voltage, ωt_0. Since none of these parameters are known to the current controller, it cannot use the exact formula to solve for the predicted grid current. A new method is needed to predict the grid current more accurately than (3) but without the computational complexity and unknown parameters required by (40). Therefore, a simple modified grid voltage value is included in (3), which takes into account that the voltage is changing over the sampling time. For the first prediction step, a modified value for $v_{g\alpha(k)}$ is needed. The arithmetic mean of $v_{g\alpha(k)}$ and $v_{g\alpha(k+1)}$ is simple to calculate and provides good approximation of the grid voltage over a sample period. The predictive formula (3) is changed to include the modified grid voltage term as follows:

$$\begin{bmatrix} i_{\alpha(k+1)} \\ i_{\beta(k+1)} \end{bmatrix} = \left(1 - R\frac{T_s}{L}\right) \begin{bmatrix} i_{\alpha(k)} \\ i_{\beta(k)} \end{bmatrix} + \frac{T_s}{L} \left(\begin{bmatrix} v_{t\alpha(k)} \\ v_{t\beta(k)} \end{bmatrix} - \frac{1}{2} \left(\begin{bmatrix} v_{g\alpha(k)} \\ v_{g\beta(k)} \end{bmatrix} + \begin{bmatrix} v_{g\alpha(k+1)} \\ v_{g\beta(k+1)} \end{bmatrix} \right) \right). \quad (41)$$

Similarly, the mean of $v_{g\alpha(k+1)}$ and $v_{g\alpha(k+2)}$ may be used for the second prediction stage. The effectiveness of this proposed modification is shown in Fig. 7(c), where minimum error is achieved where the actual parameters R and L are perfectly matched with their modeled values R_0 and L_0 and the approximate compensation method in (41) is used. Comparison between Fig. 7(c) and (b) proves that the proposed approximate compensation is equally as effective as the exact compensation but with significantly less computational burden and no reliance on unknown parameters.

VI. Stability Analysis

It is essential that the converter output current tracks the reference, therefore, the predictive control equations should be designed such that the current tracking error converges to zero. In order to prove the theoretical stability of the proposed nonlinear system in the surroundings of the steady state, the Lyapunov stability theory is used. Let there be some error between the actual grid voltage $v_{g\alpha(k)}^*$ and the voltage estimated by the modified ECKF $v_{g\alpha(k)}^e$. Similarly, let there be an error between the ideal terminal voltage, which would lead to zero error, $v_{t\alpha(k)}^*$, and the actual terminal voltage of the converter $v_{t\alpha(k)}$. Therefore

$$v_{g\alpha(k)}^* = v_{g\alpha(k)}^e + \lambda_{(k)} \quad (42)$$

$$v_{t\alpha(k)} = v_{t\alpha(k)}^* + \eta_{(k)} \quad (43)$$

where $\lambda_{(k)}$ is the grid voltage estimation error that satisfies $\|\lambda_{(k)}\| \leq \varphi$ with a constant $\varphi > 0$ and $\eta_{(k)}$ is the terminal voltage error that satisfies $\|\eta_{(k)}\| \leq \psi$ with a constant $\psi > 0$. According to (41), the future grid current is given by

$$i_{\alpha(k+1)} = \left(1 - R\frac{T_s}{L}\right) i_{\alpha(k)} + \frac{T_s}{L} \left(v_{t\alpha(k)} - \frac{1}{2} \left(v_{g\alpha(k)}^e + v_{g\alpha(k+1)}^e \right) \right) \quad (44)$$

where $v_{t\alpha(k)}$ is the actual terminal voltage of the converter and the "e" superscript denotes that these grid voltage values were estimated by the modified ECKF. Similarly, in an ideal scenario, the current reference would be tracked with zero steady-state error; therefore, the following equation can also be stated:

$$i_{\alpha(k+1)}^* = \left(1 - R\frac{T_s}{L}\right) i_{\alpha(k)} + \frac{T_s}{L} \left(v_{t\alpha(k)}^* - \frac{1}{2} \left(v_{g\alpha(k)}^* + v_{g\alpha(k+1)}^* \right) \right) \quad (45)$$

where $v_{t\alpha(k)}^*$ is the ideal converter terminal voltage to achieve zero error and $v_{g\alpha(k)}^*$ and $v_{g\alpha(k+1)}^*$ are the actual grid voltages. The current tracking error can be calculated as follows:

$$\Delta i_{(k+1)} = i_{\alpha(k+1)} - i_{\alpha(k+1)}^*. \quad (46)$$

Substituting for the actual current given by (44) and the ideal current given by (45) yields

$$\Delta i_{(k+1)} = \left[\left(1 - R\frac{T_s}{L}\right) i_{\alpha(k)} + \frac{T_s}{L} \left(v_{t\alpha(k)} - \frac{1}{2} \left(v_{g\alpha(k)}^e + v_{g\alpha(k+1)}^e \right) \right) \right] - \left[\left(1 - R\frac{T_s}{L}\right) i_{\alpha(k)} + \frac{T_s}{L} \left(v_{t\alpha(k)}^* - \frac{1}{2} \left(v_{g\alpha(k)}^* + v_{g\alpha(k+1)}^* \right) \right) \right]. \quad (47)$$

Assuming that $v_{g\alpha(k+1)}^* \approx v_{g\alpha(k)}^*$ and $v_{g\alpha(k+1)}^e \approx v_{g\alpha(k)}^e$, the future current error can be restated as

$$\Delta i_{(k+1)} = \frac{T_s}{L} \left[\left(v_{t\alpha(k)} - v_{t\alpha(k)}^* \right) + \left(v_{g\alpha(k)}^* - v_{g\alpha(k)}^e \right) \right] = \frac{T_s}{L} \left[\eta + \lambda \right]. \quad (48)$$

According to [37], a control Lyapunov function must satisfy the following stability criteria:

$$V(\Delta i_{(k)}) \geq a_1 \left|\Delta i_{(k)}\right|^l \quad \forall \Delta i_{(k)} \in G \tag{49}$$

$$V(\Delta i_{(k)}) \leq a_2 \left|\Delta i_{(k)}\right|^l \quad \forall \Delta i_{(k)} \in \Gamma \tag{50}$$

$$V(\Delta i_{(k+1)}) - V(\Delta i_{(k)}) < -a_3 \left|\Delta i_{(k)}\right|^l + a_4 \tag{51}$$

where a_1, a_2, a_3, and a_4 are positive constants, $l \geq 1$, $G \subseteq R^n$ is a positive control invariant set, and $\Gamma \subset G$ is a compact set. A Lyapunov function is proposed as

$$V_{(k)} = \frac{1}{2} \Delta i_{(k)}^T \Delta i_{(k)}. \tag{52}$$

The change of the Lyapunov function is given by

$$\Delta V_{(k)} = V_{(k+1)} - V_{(k)}. \tag{53}$$

By substituting for (48) and (52), the change in the Lyapunov can be expressed as

$$\begin{aligned} \Delta V_{(k)} = \frac{1}{2} \Bigg(\frac{T_s}{L} \Big[\left(v_{t\alpha(k)} - v^*_{t\alpha(k)} \right) \\ + \left(v^*_{g\alpha(k)} - v^e_{g\alpha(k)} \right) \Big] \Bigg)^T \Bigg(\frac{T_s}{L} \Big[\left(v_{t\alpha(k)} - v^*_{t\alpha(k)} \right) \\ + \left(v^*_{g\alpha(k)} - v^e_{g\alpha(k)} \right) \Big] \Bigg) - \frac{1}{2} \Delta i_{(k)}^T \Delta i_{(k)}. \end{aligned} \tag{54}$$

The voltage vector $v_{t\alpha(k)}$ is bounded by the available dc-link voltage. The current $i_{\alpha(k)}$ and voltage $v_{g\alpha(k)}$ are also bounded, therefore, $v^*_{t\alpha(k)}$ is bounded. By substituting for (42) and (43), the following is obtained:

$$\Delta V_{(k)} \leq -\frac{1}{2} \Delta i_{(k)}^T \Delta i_{(k)} + \frac{1}{2} \left(\frac{T_s}{L} \right)^2 (\lambda + \eta)^2 . \tag{55}$$

Therefore, the stability conditions set out in (49)–(51) are satisfied by the following constants:

$$a_1 = 1, a_2 = 1, a_3 = \frac{1}{2}, a_4 = \left(\frac{T_s}{L} \right)^2 (\lambda + \eta)^2 . \tag{56}$$

This implies that the system is stable in the sense of Lyapunov and that the current control error converges to a compact set as

$$\upsilon = \left\{ \Delta i \| \|\Delta i\| \leq \left(\frac{T_s}{L} \right) (\lambda + \eta) \right\}. \tag{57}$$

VII. Simulation Results

The effectiveness of the proposed control system is studied using MATLAB/Simulink simulations with the parameters, as shown in Table I. An MPC current controller enhanced with floating virtual voltage vectors (FVVV-MPC) was recently proposed in [20] and is used as a reference for comparison. Also, an improved MPC current controller (IMPCC) for unbalanced grids was recently proposed in [25] and is also included for comparison. Since the proposed method applies three vectors per sampling period while the IMPCC applies only one, the sampling frequency for the IMPCC is set two times higher to achieve the same switching frequency at best effort. This is consistent with the approach taken in [21], where the FCS-MPC is sampled twice as fast as the MMPC. The modified ECKF estimator is examined first, then the effectiveness of the complete control system is studied.

TABLE I
Simulation Parameters

Parameter	Symbol	Value	Unit
Nominal Grid Phase Voltage (RMS)	V_g	100	V
Grid Fundamental Frequency	f_{grid}	50	Hz
Switching Frequency (MMPC and FVVV-MPC)	f_{sw}	10	kHz
Sampling Frequency (IMPCC)	f_s	20	kHz
Voltage Measurement Noise Variance	σ_v^2	1	V
DC Link Voltage	V_{dc}	400	V
Filter Inductance	L	10	mH
Filter Resistance	R	0.1	Ω
Rated Power	P_{rated}	2	kW
Rated Current (Peak)	i_{rated}	9.428	A

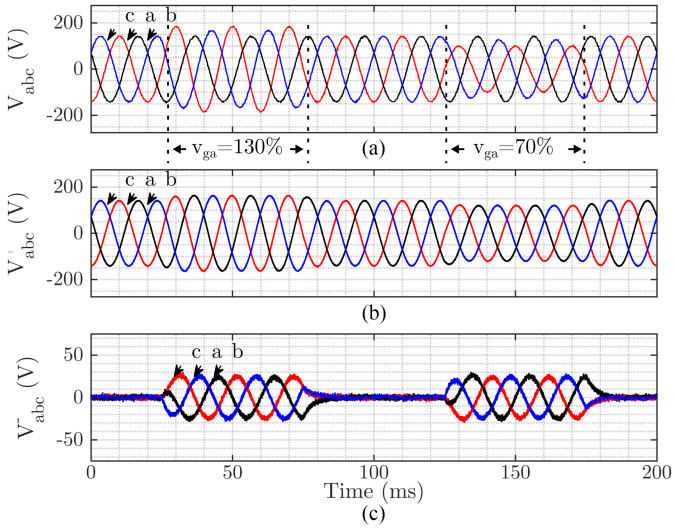

Fig. 8. Simulation results for the modified ECKF estimator. (a) Input voltage waveform corrupted by noise. (b) Estimated positive sequence component. (c) Estimated negative sequence component.

A. Modified ECKF Results

The effectiveness of the modified ECKF estimator is studied using a range of balanced and unbalanced voltage measurements corrupted by random noise.

The output of the modified ECKF estimator is shown in Fig. 8. The same simulation is run 100 times with random noise and the results are plotted on top of each other to validate the stability of the estimator in a range of random scenarios. In Fig. 8(a), the input voltage waveform is shown. In Fig. 8(b) and (c), the estimated positive and negative sequence components are shown, with the results of the 100 Monte Carlo runs superimposed. The input voltage signals are initially balanced, and the system is in steady state. At $t = 25$ ms, the magnitude of phase "a" is increased by 30%, while phase "b" remains constant and phase "c" is given by $-v_{ga(k)} - v_{gb(k)}$ in a three-wire system. At $t = 75$ ms, the input voltages return to a balanced state. At $t = 125$ ms, the magnitude of phase "a" is reduced by 30%

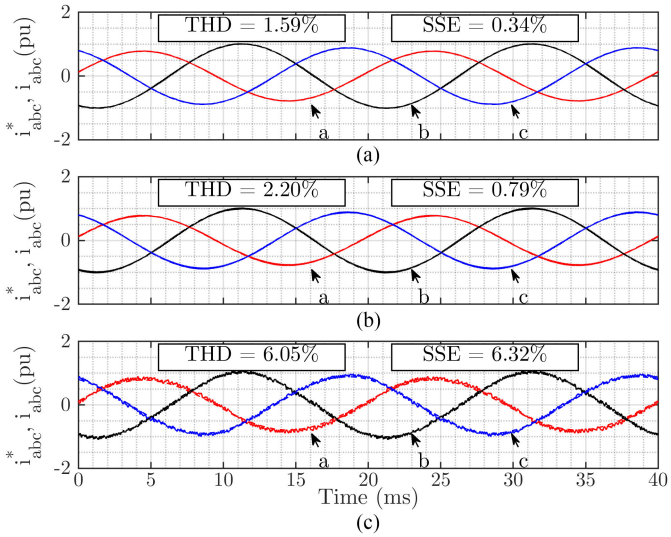

Fig. 9. Current tracking performance: (a) proposed MMPC, (b) conventional FVVV-MPC, and (c) conventional IMPCC.

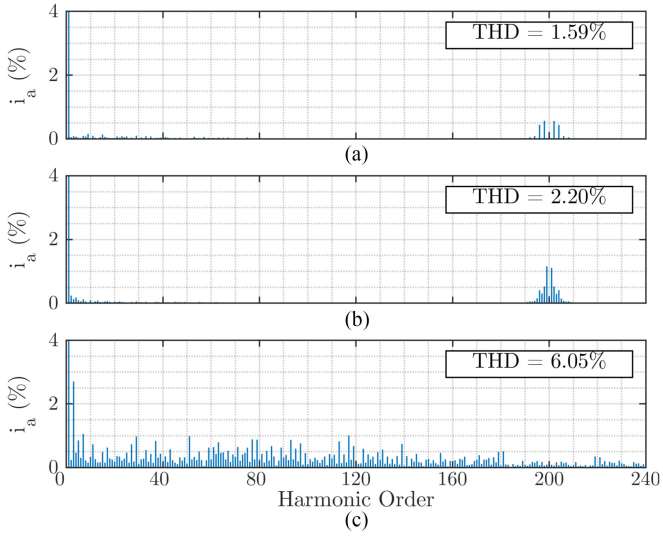

Fig. 10. Current harmonic spectrum: (a) proposed MMPC, (b) conventional FVVV-MPC, and (c) conventional IMPCC.

whilst phase "b" remains constant. Finally, at $t = 175$ ms, the input voltages return to a balanced state. The stability of the modified ECKF estimator is clearly demonstrated in Fig. 8(b) and (c), where the estimator produces a stable estimate of the positive and negative sequence components for all 100 runs. The estimator responds to step change in voltage immediately and the estimated positive sequence component settles to a new steady state in less than 2 ms. This compares favorably with conventional delayed signal techniques, which do not respond correctly for one quarter-period of the input waveform.

B. Proposed Control System

The steady-state current tracking under unbalanced conditions is studied in Fig. 9. The magnitude of phase "a" is 30% greater than phase "b," while phase "c" is given by $-v_{ga(k)} - v_{gb(k)}$. Fig. 9 shows the grid current from the proposed MMPC, the conventional FVVV-MPC and the conventional IMPCC. It can be clearly seen that the current quality is improved for the proposed MMPC, and the steady-state error is lower than both the FVVV-MPC and the IMPCC. The harmonic spectrum of the output current is studied in Fig. 10. As expected, the harmonics for the proposed MMPC and the conventional FVVV-MPC are centered around the switching frequency, while for the conventional IMPCC, there is a spread spectrum of harmonic content. The THD for the proposed controller is 1.59% whilst for the FVVV-MPC it is 2.20% and for the IMPCC controller it is 6.05%; therefore, a significant improvement in power quality has been achieved. The transient performance of the current controller is also studied during a step change in active power reference from zero to rated power at unity power factor. Fig. 11 shows the active and reactive power of all three controllers during the step change. The IMPCC benefits from a higher sampling frequency; however, the proposed MMPC benefits from overmodulation capability, therefore, the proposed controller offers the comparable transient performance

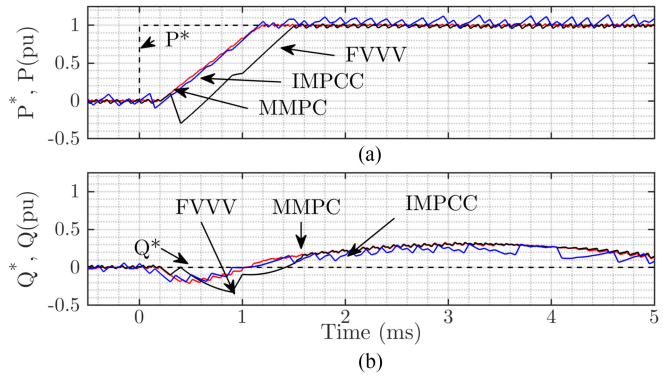

Fig. 11. Dynamic active and reactive power tracking for the proposed MMPC, conventional FVVV-MPC, and conventional IMPCC: (a) active power and (b) reactive power.

TABLE II
CONTROLLER COMPARISON

Criteria	Proposed MMPC	FVVV-MPC [20]	IMPCC [25]
THD	Lowest	Low	High
SSE	Lowest	Low	High
Transient Response	Fast	Slow	Fast
Power Ripple	Lowest	Low	High

to the conventional IMPCC. The FVVV-MPC does not benefit from the increased sampling frequency of the IMPCC nor the overmodulation capability of the proposed MMPC; therefore, its transient performance is slower. The proposed MMPC with its improved current quality offers the lowest power ripple. The advantages and disadvantages of the proposed MMPC, conventional FVVV-MPC, and conventional IMPCC are summarized in Table II.

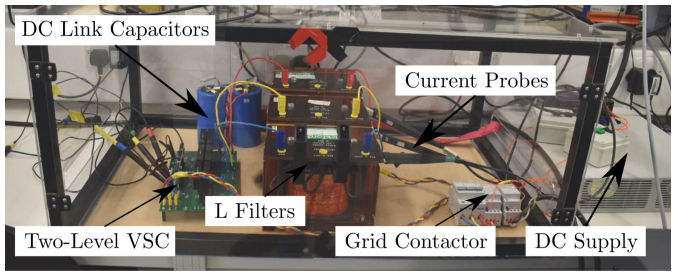

Fig. 12. Hardware test rig.

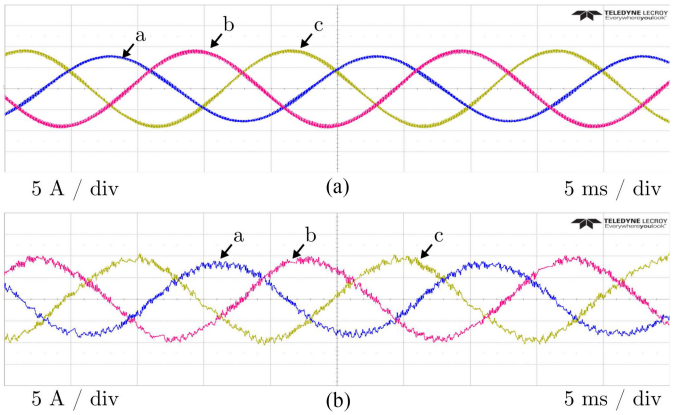

Fig. 13. Current tracking performance: (a) proposed MMPC and (b) conventional IMPCC.

VIII. Experimental Validation

The proposed MMPC was implemented in the laboratory to verify the performance of the control system. Since conventional finite-set MPC is more prevalent in the literature than virtual-vector-based MPC due to its faster response, the IMPCC was selected for comparison in the experiments. The experimental test rig is shown in Fig. 12 and the system parameters are as shown in Table I. The steady-state current tracking under unbalanced conditions is studied in Fig. 13. The magnitude of phase voltage "a" is 30% greater than phase "b," while phase "c" is given by $-v_{ga(k)} - v_{gb(k)}$. Fig. 13 shows the experimental results for the proposed MMPC and the IMPCC. The current quality is improved for the proposed MMPC compared with the IMPCC technique. The harmonic spectrum of the experimental output currents is shown in Fig. 14. The harmonics for the proposed MMPC are centered around the switching frequency, while for the conventional IMPCC, there is a spread spectrum of harmonic content. The THD for the proposed controller is 2.47% while for the conventional controller it is 5.4%. This is close to the simulation result.

Fig. 15 shows the outputs of the proposed controller in a range of scenarios. Fig. 15(a) shows the calculated active and reactive power at full rated power in a balanced grid, with currents, as shown in Fig. 15(b). Fig. 15(c) shows the calculated powers where the phase "a" voltage is increased by 30% and the negative sequence voltage is not compensated. The resulting balanced currents are shown in Fig. 15(d). Finally, Fig. 15(e) shows the

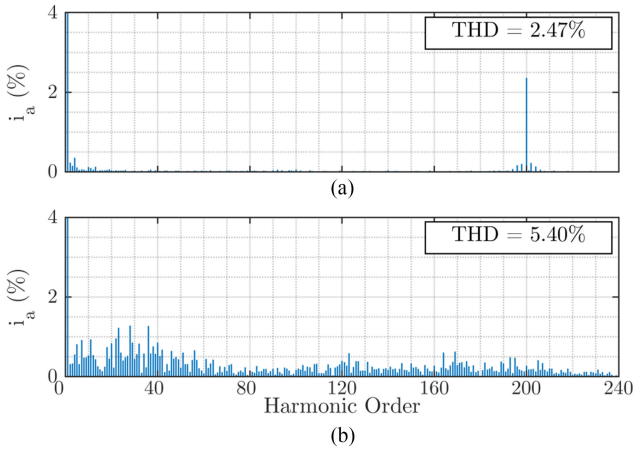

Fig. 14. Experimental current harmonic spectrum: (a) proposed MMPC and (b) conventional IMPCC.

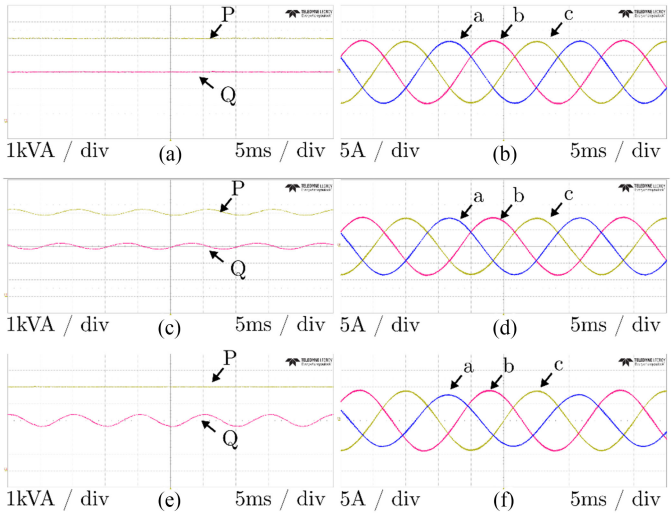

Fig. 15. Experimental results for the proposed controller: (a) PQ in balanced grid, (b) currents in balanced grid, (c) PQ in unbalanced grid without compensation, (d) currents in unbalanced grid without compensation, (e) PQ in unbalanced grid with compensation, and (f) currents in unbalanced grid with compensation.

calculated powers where the phase "a" voltage is increased by 30% and the negative sequence component is compensated by the modified ECKF estimator. The resulting unbalanced currents are shown in Fig. 15(f). The effectiveness of the proposed controller is clearly demonstrated. Near zero steady-state error is achieved under balanced and unbalanced operation and constant active power is exported to the grid with high power quality. The transient performance of both current controllers is also studied in experiment during a step change in active power reference from zero to rated power at unity power factor. Fig. 16 shows the active and reactive power of both controllers during the step change. Both controllers have similar responses; however, the proposed MMPC has superior the steady-state performance, with reduced ripple in the active power. Finally, the behavior of both controllers is studied during a step change from zero to rated power at unity power factor, as shown in Fig. 17. Both

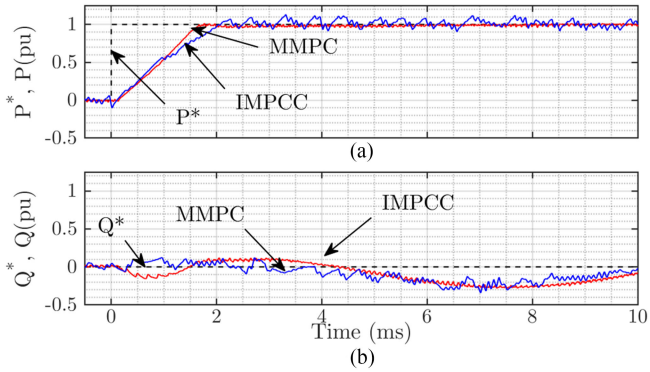

Fig. 16. Dynamic active and reactive power tracking: (a) proposed MMPC controller and (b) conventional IMPCC.

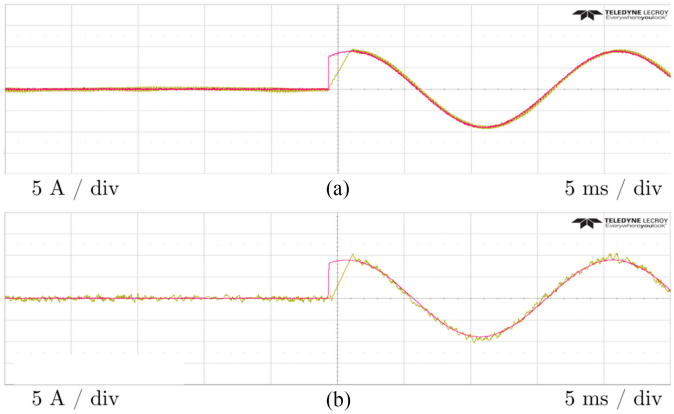

Fig. 17. Phase "a" current during step change from zero to full rated power: (a) proposed MMPC and (b) conventional IMPCC.

controllers track the reference quickly, achieving a steady state in 2.5 ms, however, the proposed MMPC achieves a higher current quality, as shown in Fig. 17(a).

IX. Computational Burden

The MMPC controller proposed in this article and the conventional IMPCC were implemented in the laboratory using a Texas Instruments TMS320F28379D microcontroller. The execution times for the two techniques are shown in Fig. 18. The execution time of the proposed controller is 12.5 μs, while the execution time of the conventional IMPCC controller is 13 μs. To achieve a minimum switching frequency of 10 kHz, the IMPCC must be executed twice per switching period, meaning that only 37μs is available to include any extra control algorithms to achieve the minimum switching frequency of 10 kHz. In comparison, the proposed MMPC offers 87.5 μs of additional time. In summary, the proposed MMPC has twice the available extra program execution time compared with the conventional IMPCC to achieve the same switching frequency. For example, if it is required to design a converter with higher switching frequency, such as 40 kHz, then the proposed MMPC can be used but the conventional IMPCC cannot.

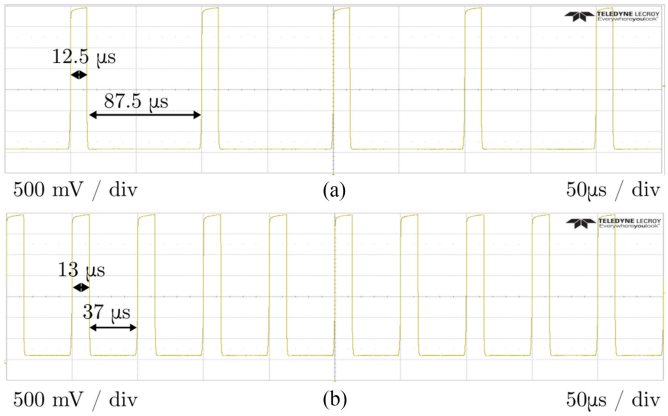

Fig. 18. Execution time: (a) proposed controller and (b) existing IMPCC controller.

X. Conclusion

In this article, a new model predictive current controller has been proposed for unbalanced grids. The variable switching frequency problem of conventional MPC has been addressed in a computationally efficient way. The ECKF estimator, which has been proposed previously for protection purposes, is also extended to the new application of current control and its suitability for this purpose has been proven. The ECKF has also been modified to provide a new calculation time compensation technique offering superior accuracy to the well-known Lagrange technique, and a grid voltage discretization compensation strategy is outlined. The proposed controller has been studied in simulation and validated experimentally. Simulation and practical results have confirmed the excellent performance of the system compared with existing approaches. Low steady-state error and high power quality are achieved and a fast transient response is provided.

References

[1] J. Zhao, M. Huang, H. Yan, C. K. Tse, and X. Zha, "Nonlinear and transient stability analysis of phase-locked loops in grid-connected converters," *IEEE Trans. Power Electron.*, vol. 36, no. 1, pp. 1018–1029, Jan. 2021.

[2] L. Huang *et al.*, "Grid-synchronization stability analysis and loop shaping for PLL-based power converters with different reactive power control," *IEEE Trans. Smart Grid*, vol. 11, no. 1, pp. 501–516, Jan. 2020.

[3] F. Sadeque, J. Benzaquen, A. Adib, and B. Mirafzal, "Direct phase-angle detection for three-phase inverters in asymmetrical power grids," *IEEE Trans. Emerg. Sel. Topics Power Electron.*, vol. 9, no. 1, pp. 520–528, Feb. 2021.

[4] A. Timbus, M. Liserre, R. Teodorescu, P. Rodriguez, and F. Blaabjerg, "Evaluation of current controllers for distributed power generation systems," *IEEE Trans. Power Electron.*, vol. 24, no. 3, pp. 654–664, Mar. 2009.

[5] Y. Zhang, T. Jiang, and J. Jiao, "Model-free predictive current control of DFIG based on an extended state observer under unbalanced and distorted grid," *IEEE Trans. Power Electron.*, vol. 35, no. 8, pp. 8130–8139, Aug. 2020.

[6] K. H. Ahmed, A. M. Massoud, S. J. Finney, and B. W. Williams, "A synchronous DQ frame controller via an LCL coupled filter under unbalanced three-phase voltage supply conditions," in *Proc. Int. Conf. Power Eng. Energy Electr. Drives*, 2011, pp. 1–6.

[7] R. Teodorescu, M. Liserre, and P. Rodriguez, *Grid Synchronization in Three Phase Power Converters*. Hoboken, NJ, USA:Wiley, 2007, pp. 169–204.

[8] D. Zhu, S. Zhou, X. Zou, and Y. Kang, "Improved design of PLL controller for LCL-type grid-connected converter in weak grid," *IEEE Trans. Power Electron.*, vol. 35, no. 5, pp. 4715–4727, May 2020.
[9] X. Li and H. Lin, "A design method of phase-locked loop for grid-connected converters considering the influence of current loops in weak grid," *IEEE Trans. Emerg. Sel. Topics Power Electron.*, vol. 8, no. 3, pp. 2420–2429, Sep. 2020.
[10] A. K. Verma, R. K. Jarial, P. Roncero-Sánchez, M. R. Ungarala, and J. M. Guerrero, "An improved hybrid prefiltered open-loop algorithm for three-phase grid synchronization," *IEEE Trans. Ind. Electron.*, vol. 68, no. 3, pp. 2480–2490, Mar. 2021.
[11] J. Rodriguez and P. Cortes, *Predictive Control of a Three-Phase Inverter*. Hoboken, NJ, USA: Wiley, 2012, pp. 41–63.
[12] A. Sarajian *et al.*, "Overmodulation methods for modulated model predictive control and space vector modulation," *IEEE Trans. Power Electron.*, vol. 36, no. 4, pp. 4549–4559, Apr. 2021.
[13] S. A. Hossain and M. Habibullah, "Modulated model predictive current control of three-level NPC inverter with overmodulation capability," in *Proc. 11th Int. Conf. Elect. Comput. Eng.*, 2020, pp. 137–140.
[14] T. Sun *et al.*, "Improved modulated model-predictive control for PMSM drives with reduced computational burden," *IET Power Electron.*, vol. 13, no. 14, pp. 3163–3170, Nov. 2020.
[15] Y. Yang, H. Wen, and D. Li, "A fast and fixed switching frequency model predictive control with delay compensation for three-phase inverters," *IEEE Access*, vol. 5, pp. 17904–17913, 2017.
[16] Y. Zhang and W. Xie, "Low complexity model predictive control-single vector-based approach," *IEEE Trans. Power Electron.*, vol. 29, no. 10, pp. 5532–5541, Oct. 2014.
[17] Y. Zhang, W. Xie, Z. Li, and Y. Zhang, "Low-complexity model predictive power control: Double-vector-based approach," *IEEE Trans. Ind. Electron.*, vol. 61, no. 11, pp. 5871–5880, Nov. 2014.
[18] Y. Zhang, Y. Peng, and H. Yang, "Performance improvement of two-vectors-based model predictive control of PWM rectifier," *IEEE Trans. Power Electron.*, vol. 31, no. 8, pp. 6016–6030, Aug. 2016.
[19] S. Vazquez *et al.*, "Model predictive control with constant switching frequency using a discrete space vector modulation with virtual state vectors," in *Proc. IEEE Int. Conf. Ind. Technol.*, 2009, pp. 1–6.
[20] P. Falkowski, A. Sikorski, and M. Malinowski, "Finite control set model predictive control with floating virtual voltage vectors for grid-connected voltage source converter," *IEEE Trans. Power Electron.*, vol. 36, no. 10, pp. 11875–11885, Oct. 2021.
[21] L. Tarisciotti, P. Zanchetta, A. Watson, J. C. Clare, M. Degano, and S. Bifaretti, "Modulated model predictive control for a three-phase active rectifier," *IEEE Trans. Ind. Appl.*, vol. 51, no. 2, pp. 1610–1620, Mar./Apr. 2015.
[22] C. F. Garcia, C. A. Silva, J. R. Rodriguez, P. Zanchetta, and S. A. Odhano, "Modulated model-predictive control with optimized overmodulation," *IEEE Trans. Emerg. Sel. Topics Power Electron.*, vol. 7, no. 1, pp. 404–413, Mar. 2019.
[23] L. H. B. Liboni, M. C. de Oliveira, and I. N. D. Silva, "Optimal kalman estimation of symmetrical sequence components," *IEEE Trans. Instrum. Meas.*, vol. 69, no. 11, pp. 8844–8852, Nov. 2020.
[24] N. Jin, L. Guo, C. Gan, S. Hu, and Z. Dou, "Finite-state model predictive power control of three-phase bidirectional AC/DC converter under unbalanced grid faults with current harmonic reduction and power compensation," *IET Power Electron.*, vol. 11, no. 2, pp. 348–356, 2018.
[25] N. Jin, C. Gan, and L. Guo, "Predictive control of bidirectional voltage source converter with reduced current harmonics and flexible power regulation under unbalanced grid," *IEEE Trans. Energy Convers.*, vol. 33, no. 3, pp. 1118–1131, Sep. 2018.
[26] D. Sun and X. Wang, "Low-complexity model predictive direct power control for DFIG under both balanced and unbalanced grid conditions," *IEEE Trans. Ind. Electron.*, vol. 63, no. 8, pp. 5186–5196, Aug. 2016.
[27] T. Hao, F. Gao, and T. Xu, "Fast symmetrical component extraction from unbalanced three-phase signals using non-nominal dq-transformation," *IEEE Trans. Power Electron.*, vol. 33, no. 11, pp. 9134–9141, Nov. 2018.
[28] A. Rahoui, A. Bechouche, H. Seddiki, and D. Ould Abdeslam, "Virtual flux estimation for sensorless predictive control of PWM rectifiers under unbalanced and distorted grid conditions," *IEEE Trans. Emerg. Sel. Topics Power Electron.*, vol. 9, no. 2, pp. 1923–1937, Apr. 2021.
[29] J. Kukkola and M. Hinkkanen, "State observer for grid-voltage sensorless control of a converter under unbalanced conditions," *IEEE Trans. Ind. Appl.*, vol. 54, no. 1, pp. 286–297, Jan./Feb. 2018.
[30] R. A. Fantino, C. A. Busada, and J. A. Solsona, "Observer-based grid-voltage sensorless synchronization and control of a VSI-LCL tied to an unbalanced grid," *IEEE Trans. Ind. Electron.*, vol. 66, no. 7, pp. 4972–4981, Jul. 2019.
[31] L. Guo, N. Jin, Y. Li, and K. Luo, "A model predictive control method for grid-connected power converters without AC voltage sensors," *IEEE Trans. Ind. Electron.*, vol. 68, no. 2, pp. 1299–1310, Feb. 2021.
[32] H. Yang, Y. Zhang, J. Liang, J. Gao, P. D. Walker, and N. Zhang, "Sliding-mode observer based voltage-sensorless model predictive power control of PWM rectifier under unbalanced grid conditions," *IEEE Trans. Ind. Electron.*, vol. 65, no. 7, pp. 5550–5560, Jul. 2018.
[33] A. T. Phan, G. Hermann, and P. Wira, "Kalman filtering with a new state-space model for three-phase systems: Application to the identification of symmetrical components," in *Proc. IEEE Int. Conf. Evolving Adaptive Intell. Syst.*, 2015, pp. 1–6.
[34] Z. Tang, L. Du, L. Xiong, M. Li, X. Ma, and G. Tang, "A fast extraction of positive sequence components with noise immunity in unbalanced conditions," in *Proc. IEEE Power Energy Soc. Gen. Meeting*, 2020, pp. 1–5.
[35] W. Lei, W. Jiang, Y. Wang, and H. Huang, "Different control objectives under stationary frame for grid-connected converter under unbalanced grid voltage," in *Proc. IEEE 8th Int. Power Electron. Motion Control Conf.*, 2016, pp. 725–730.
[36] H. A. Young, M. A. Perez, and J. Rodriguez, "Analysis of finite-control-set model predictive current control with model parameter mismatch in a three-phase inverter," *IEEE Trans. Ind. Electron.*, vol. 63, no. 5, pp. 3100–3107, May 2016.
[37] R. P. Aguilera and D. E. Quevedo, "On stability and performance of finite control set MPC for power converters," in *Proc. Workshop Predictive Control Elect. Drives Power Electron.*, 2011, pp. 55–62.

Euan T. Andrew (Student Member, IEEE) received the B.Eng. (first class Hons.) degree in electronic and electrical engineering from the University of Strathclyde, Glasgow, U.K., in 2018. He is currently working toward the Ph.D. degree in electronic and electrical engineering with the University of Strathclyde, Glasgow, U.K.

His current research interests include modeling of grid-connected power converters and the design of switch-mode power supplies with embedded microprocessor control.

Khaled H. Ahmed (Senior Member, IEEE) received the B.Sc.(Hons.) and M.Sc. degrees from Alexandria University, Alexandria, Egypt, in 2002 and 2004, respectively, and the Ph.D. degree in power electronics applications from the University of Strathclyde, Glasgow, U.K., in 2008.

He was a Professor with Alexandria University, in 2019. He is currently a Reader in Power Electronics with the University of Strathclyde. He has authored or coauthored more than 140 technical articles in refereed journals and conferences as well as a published textbook titled *High Voltage Direct Current Transmission: Converters, Systems and DC Grids* (Wiley, 2015), a book chapter contribution, and holds a PCT patent PCT/GB2017/051364. His research interests include renewable energy integration, high-power converters, offshore wind energy, dc/dc converters, HVdc, and smart grids.

Dr. Ahmed is a Senior Member of the IEEE Power Electronics Society and the IEEE Industrial Electronics Society.

Derrick Holliday received the Ph.D. degree from Heriot-Watt University, Edinburgh, U.K., in 1995.

He was with the University of Bristol, Bristol, U.K., and the University of Strathclyde, Glasgow, U.K. He is currently leading industrially funded research in the field of power electronics for HVdc applications and is a coinvestigator on research programs in the fields of photovoltaic systems and the interface of renewable energy to HVdc systems. He has authored or coauthored more than 70 academic journal and conference publications. His research interests include the areas of power electronics, electrical machines, and drives.